Published in final edited form as:
J Am Chem Soc. 2010 October 27; 132(42): 14877–14885. doi:10.1021/ja105312p.

Hydride-Containing Models for the Active Site of the Nickel-Iron Hydrogenases

Bryan E. Barton and **Thomas B. Rauchfuss**
School of Chemical Sciences University of Illinois at Urbana-Champaign Urbana, IL 61801

Abstract

The [NiFe]-hydrogenase model complex NiFe(pdt)(dppe)$(CO)_3$ (**1**) (pdt = 1,3-propanedithiolate) has been efficiently synthesized and found to be robust. This neutral complex sustains protonation to give the first nickel-iron hydride [**1**H]BF_4. One CO ligand in [**1**H]BF_4 is readily substituted by organophosphorus ligand to afford the substituted derivatives [HNiFe(pdt)(dppe)$(CO)_2(PR_3)$]BF_4, where PR_3 = $P(OPh)_3$ ([**2**H]BF_4); PPh_3 ([**3**H]BF_4); PPh_2Py ([**4**H]BF_4, where Py = 2-pyridyl). Variable temperature NMR measurements show that the neutral and protonated derivatives are dynamic on the NMR timescale, which partially symmetrizes the phosphine complex. The proposed stereodynamics involve twisting of the Ni(dppe) center, not rotation at the $Fe(CO)_2(PR_3)$ center. In MeCN solution, **3**, which can be prepared by deprotonation of [**3**H]BF_4 with NaOMe, is about 10^4 stronger base than is **1**. X-ray crystallographic analysis of [**3**H]BF_4 revealed a highly unsymmetrical bridging hydride, the Fe-H bond being 0.40 Å shorter than the Ni-H distance. Complexes [**2**H]BF_4, [**3**H]BF_4, [**4**H]BF_4 undergo reductions near −1.46 V vs $Fc^{0/+}$. For [**2**H]BF_4, this reduction process is reversible, and we assign it as a one-electron process. In the presence of trifluoroacetic acid, proton reduction catalysis coincides with this reductive event. The dependence of i_c/i_p on the concentration of the acid indicates that H_2 evolution entails protonation of a reduced hydride. For [**2**H]$^+$, [**3**H]$^+$, and [**4**H]$^+$, the acid-independent rate constants are 50-75 s^{-1}. For [**2**H]$^+$ and [**3**H]$^+$, the overpotentials for H_2 evolution are ~430 mV, whereas the overpotential for the *N*-protonated pyridinium complex $[\mathbf{4}H_2]^{2+}$ is estimated to be 260 mV. The mechanism of H_2 evolution is proposed to follow an ECEC sequence, where E and C correspond to one-electron reductions and protonations, respectively. On the basis of their values for its pK_a and redox potentials, $\Delta G_{H\bullet}$ and ΔG_{H^-} are 57 and 79 kcal/mol for [**1**H]$^+$ and [**1**]$^{2+}$, respectively.

Introduction

Two families of hydrogenases, the [FeFe]-hydrogenases and the [NiFe]-hydrogenases,[2-4] have stimulated intense work on the development of bioinspired catalysts for hydrogen processing.[5,6] In the case of the [FeFe]-hydrogenases, the transition from structural to functional model complexes was rapid owing to foundational work conducted, albeit without awareness of the biological connection,[7] years before the structural characterization of these proteins. Modeling the [NiFe]-hydrogenases has proven more challenging, despite the fact that the relevant proteins had been structurally characterized already in the 1990's. Relative to the [FeFe]-enzymes, the [NiFe]-hydrogenases are well suited for modeling since these protein are diverse,[8] sometimes oxygen-tolerant,[9] and are catalytic biased for H_2 oxidation,[10] which is the more challenging reaction for model complexes.

Supporting Information Available: Spectra, electrochemical data, and illustrative calculations. Crystallographic information file (cif) for [**3**H]BF_4. This material is available free of charge via the Internet at http://pubs.acs.org.

Diverse structural models for the [NiFe]-hydrogenases have been described,11 including many that feature $Ni(SR)_2Fe$ cores complemented by diatomic ligands on Fe.12 Unlike model complexes for the active site of the [FeFe]-hydrogenases, where hydrides are numerous, active site models for the [NiFe]-enzymes have until recently lacked hydride ligands.13,14 Our contributions to this area of active site modeling have focused on developing strategies for installing hydride ligands. For example, one could attach Ni modules to substitutionally labile iron hydrides and, complementarily, attach Fe species to Ni hydrides. We have investigated the former route with partial success. The species $[HFe(CN)_2(CO)_3]^-$, which contains a biomimetic ferrous $[HFe(CO)(CN)_2]^-$ module, has been prepared efficiently.15 Although $[HFe(CN)_2(CO)_3]^-$ undergoes well-behaved substitution reactions, it has not yet been condensed with nickel thiolates. Alternatively, we envisioned reactions of preformed $Ni(SR)_2Fe$ ensembles with the equivalent of H^- or H^+. Hydrides can be installed on diferrous dithiolates using BH_4^- salts.16 We have generated impure samples of $[(dppe)Ni(\mu\text{-}pdt)(\mu\text{-}H)Fe(CO)(dppe)]^+$ from $[(dppe)Ni(\mu\text{-}pdt)Fe(CO)_2(dppe)]^{2+}$ via this method (dppe = 1,2-bis(diphenylphosphino)ethane, pdt = 1,3-propanedithiolate).14

The final approach to nickel-iron hydrides calls for protonation of reduced $Ni(SR)_2Fe$ species, a route that is analogous to well developed in the modeling of the [FeFe]-hydrogenases.17 Most structural models feature $Ni^{II}(SR)_2Fe^{II}$ cores, but a few consist of $L_2(RS)Ni^{II}(SR)Fe^0(CO)_4$ centers, which in principle could be protonated at iron.18 Despite its reputed instability, the $Ni^I(SR)_2Fe^I$ species $(dppe)Ni(\mu\text{-}pdt)Fe(CO)_3$ (**1**) was attractive to us.19 We found that protonation of **1** efficiently affords $[(dppe)Ni(\mu\text{-}pdt)(\mu\text{-}H)Fe(CO)_3]^+$ ($[\mathbf{1}H]^+$), the first hydride-containing model for the [NiFe]-hydrogenases. This heterobimetallic hydride resembles the active site with respect to the presence of a $L_2Ni(H)(SR)_2Fe(CO)L_2$ core, although it diverges from the biological structure in other ways. The finding that $[\mathbf{1}H]^+$ is an active catalyst for proton reduction demonstrated that even approximate models could prove functional, a finding that underscores the importance of hydride ligands in modeling of the hydrogenases.13 In this paper we describe progress in modifying the $Fe(CO)_3$ subsite and the chemical consequences thereof. The resulting derivatives are highly amenable to analysis of key design features, including stereodynamics, basicity, and proton relay.

Results and Discussion

NiFe(pdt)(dppe)(CO)$_3$ and Hydride Derivatives

Complex **1** has been characterized crystallographically by Schröder *et al*.19 The physical properties of our samples differ from that previously reported.19 The $31P\{^1H\}$ NMR spectrum consists of a broadened singlet at room temperature that decoalesces into two doublets at −68 °C. This pattern is consistent with rotation of the trigonal bipyramidal Ni(dppe) site (Scheme 1).

Treatment of a CH_2Cl_2 solution **1** with $HBF_4{\bullet}Et_2O$ or CF_3COOH resulted in immediate protonation to yield the respective salts of the cationic hydride. The tetrafluoroborate salt ($[\mathbf{1}H]BF_4$) was isolated as a stable red microcrystalline solid that is soluble in CH_2Cl_2, THF, MeCN, and MeOH. Its $^{31}P\{^1H\}$ NMR spectrum displays a sharp singlet at δ 71. In the ^1H NMR spectrum, the hydride signal appears as a triplet of triplets (J = 6, 0.6 Hz, Figure 1). The 6 Hz coupling is a typical J_{PH} for nickel phosphine hydrides, e.g. J_{PH} = 6 Hz for $[HNi(dppe)_2]AlCl_4$.20 The smaller coupling, confirmed by the $\{^1H\text{-}^1H\}$ COSY spectrum, arises from coupling to protons on the dithiolate. The same cationic hydride can be generated from H_2 in the presence of the borane $B(C_6F_5)_3$21 (eq 1).

$$\mathrm{NiFe(pdt)(dppe)(CO)_3 + H_2 + B(C_6F_5)_3 \rightarrow [HNiFe(pdt)(dppe)(CO)_3]HB(C_6F_5)_3} \quad (1)$$

Mono-substituted complexes $[HNiFe(pdt)(dppe)(PR_3)(CO)_2]BF_4$ were prepared via thermal and photochemical substitution of [**1**H]BF_4 (eq 2).

$$\mathrm{[HNiFe(pdt)(dppe)(CO)_3]BF_4 + L \rightarrow} \begin{array}{l} \mathrm{[HNiFe(pdt)(dppe)(L)(CO)_2]BF_4 + CO} \\ \mathrm{[2H]BF_4,\ L = P(OPh)_3} \\ \mathrm{[3H]BF_4,\ L = PPh_3} \\ \mathrm{[4H]BF_4,\ L = PPh_2Py} \end{array} \quad (2)$$

FT-IR spectra of these adducts feature a pair of comparably intense ν_{CO} bands at about 2025 and 1970 cm^{-1} (Figure 2). The positions of these bands indicate the expected sequence of basicity, i.e. $P(OPh)_3 < PPh_2Py < PPh_3$. The ^1H NMR spectra exhibited doublet of triplets (J_{PH} ~ 35, 4 Hz) in the hydride region, the coupling to the dppe ligands being slightly less than that of the tricarbonyl hydride, [**1**H]BF_4. In addition, all three monosubstituted hydrides displayed an additional doublet of triplets (J_{PH} ~ 40, 5 Hz) accounting for ~1% of the sample (see Figure 1). The identity of this second species is unknown, but we suggest that it is an isomer. Such a species is observed in the spectra for [**2**H]$^+$, [**3**H]$^+$, and [**4**H]$^+$, but its NMR shift varies with the identity of the phosphorous ligand.

Variable temperature $^{31}P\{^1H\}$ NMR spectra provide insights into the dynamics that cannot be readily obtained for the more symmetrical [**1**H]BF_4. The signal assigned to dppe (δ 65) was broad at room temperature but decoalesced at −60 °C into two doublets. The singlet for PPh_3 remained unchanged throughout this experiment (Figure 3). This DNMR pattern is consistent with both (i) a rocking of the $Fe(PPh_3)(CO)_2$ subunit between two equivalent structures (Scheme 2) and rotation of the Ni(dppe) center. We have previously shown that related diiron dithiolates, e.g. $Fe_2(pdt)(CO)_4$(diphosphine) are subject to a degenerate rocking interchange of the basal sites.22 Variable temperature ^{13}C NMR spectra show that the P*C*H_2*C*H_2P signals (Δν = 180 Hz at −60 °C) are fully coalesced at +19 °C, but the S*C*H_2 signals (Δν = 91 Hz at −30 °C) remain completely distinct. The finding that more closely spaced S*C*H_2 signals coalesce at higher temperatures than the P*C*H_2*C*H_2P signals is inconsistent with the rocking of the $Fe(CO)_2PPh_3$ group. Thus rotation of the Ni(dppe) center proceeds with a lower barrier.

Complex [**3**H]BF_4 was further characterized by X-ray crystallography, which confirmed that PPh_3 is *cis* to the hydride (Figure 4). The Fe(1)-Ni(1) distance of 2.6432(7) Å is only slightly longer than that of [**1**H]BF_4 (2.6131(14) Å). The Fe-Ni distance in the *D. vulgaris* enzyme for the Ni-C/Ni-R state is 2.55 Å.2 The bridging hydride position for [**3**H]BF_4 is unsymmetrical, closer to iron than nickel by 0.40 Å, whereas in [**1**H]BF_4 the hydride ligand is closer to iron by only 0.18 Å. The unsymmetrical character of the hydride ligand is also indicated by the diminished value of J_{dppeH}. The Fe(1)-S(1)-Ni(1) angle in [**3**H]BF_4 (71.42(3)°) is almost identical to that for [**1**H]BF_4 (70.39(6)°). The OC-Fe-CO angle is ~ 99°, vs the value of 96° calculated from the difference in the intensities of the two ν_{CO} bands.23

$NiFe(pdt)(dppe)(PPh_3)(CO)_2$ (**3**) can be prepared in analytical purity by the deprotonation of [**3**H]BF_4 with NaOMe. The ν_{CO} bands of **3** (CH_2Cl_2: 1971, 1916 cm^{-1}) shift by about 45 cm^{-1} toward lower energy (Figure 5). The $^{31}P\{^1H\}$ NMR spectrum (Figure 6) of a CD_2Cl_2 solution at room temperature displays a triplet (δ 55) assigned to the PPh_3 ligand and two broad signals for the dppe (δ 77, 45). Upon cooling the sample to −20 °C, the dppe signals

sharpen to the expected AB quartet and the PPh_3 signal appears as a doublet-of-doublets. This dynamic behavior is analogous to that proposed for **1**.

The pyridylphosphine hydride $[\mathbf{4}H]^+$ displays more complexity than $[\mathbf{2}H]^+$ and $[\mathbf{3}H]^+$. Addition of D_2O to a d^6-acetone solution of $[\mathbf{4}H]BF_4$ in CD_2Cl_2 solution resulted in conversion to $[\mathbf{4}D]BF_4$ within seconds. Under the same conditions the corresponding PPh_3 derivative $[\mathbf{3}H]BF_4$ was found to exchange only slowly ($t_{1/2}$ = 20 min). Similarly, $[\mathbf{4}H]BF_4$ was rapidly deprotonated by NEt_3, whereas treatment of excess NEt_3 to the analogous PPh_3 derivative required hours under comparable conditions.

$$\text{fast:}\quad [4H]BF_4 + D_2O \rightarrow [4D]BF_4 + HOD$$
$$\text{slow:}\quad [3H]BF_4 + D_2O \rightarrow [3D]BF_4 + HOD$$

The IR spectrum of $[\mathbf{4}H]BF_4$ is more complex than that for $[\mathbf{2}H]BF_4$ and is indicative of a mixture of three equilibrating species. In THF solution, bands are observed not only for the expected cationic hydride $[\mathbf{4}H]^+$, but also for neutral **4** and the *N*-protonated hydride $[\mathbf{4}H_2]^{2+}$. At room temperature, the relative amounts of the organometallic components in the solution were estimated by simulation of the IR spectrum, giving K_{prot} (eq 3).

$$K_{prot} = ([4])\left(\left[4H_2{}^{2+}\right]\right)/([4H]^+)^2 \sim 0.03 \tag{3}$$

Addition of excess CF_3CO_2H to a CH_2Cl_2 solution of $[\mathbf{4}H]^+$ gave a new hydride with a concomitant increase of ν_{CO} by ~10 cm^{-1}. This shift is consistent with protonation of the pyridine ligand giving $[\mathbf{4}H_2]^{2+}$ (eq 4). The ^1H NMR spectrum of $[\mathbf{4}H_2]^{2+}$ features a doublet of triplets centered at δ = − 3.11 (J_{PH} = 40, 3.5 Hz). The $^{31}P\{^1H\}$ NMR spectrum resembles that for $[\mathbf{3}H]BF_4$, suggesting that the overall structure of the hydride remains unchanged. Consistent with the weak donor ability of PPh_2PyH^+, $[\mathbf{4}H_2]^{2+}$ is not stable for prolonged periods of time or in the presence of excess acid and degrades to $[\mathbf{1}H]^+$, and free phosphine.

$$[HNiFe(pdt)(dppe)(PPh_2Py)(CO)_2]^+ + CF_3CO_2H \rightarrow [HNiFe(pdt)(dppe)(PPh_2PyH)(CO)_2]^{2+}[4H_2]^{2+} \tag{4}$$

Redox Properties and Catalytic Hydrogen Evolution

Cyclic voltammetry indicates that the complexes $[\mathbf{1}H]BF_4$, $[\mathbf{2}H]BF_4$, $[\mathbf{3}H]BF_4$, undergo at least quasi-reversible reductions at about −1.5 V (Table 1). The corresponding reduction for $[\mathbf{4}H]BF_4$ was irreversible. For complex $[\mathbf{2}H]BF_4$, this couple was highly reversible with i_{pa}/i_{pc} of 0.93 A one-electron process for the reduction of $[\mathbf{2}H]^+$ is also indicated by ΔE_p ~65 mV. Additionally, the scan rate dependence for the $[\mathbf{2}H]^{+/0}$ and $[\mathbf{2}]^{0/+}$ couples are very similar. We have independently established the one-electron nature of the oxidation of **2** to give the mixed-valence $Ni^{II}Fe^{I}$ complex (Figure 7).24 The oxidation of CH_2Cl_2 solutions of $[\mathbf{2}H]BF_4$, $[\mathbf{3}H]BF_4$, and $[\mathbf{4}H]BF_4$ occur at ~ 0.5 V vs $Fc^{0/+}$ and are irreversible.

Upon addition of CF_3CO_2H (pK_a^{MeCN} = 12.65,25 $E°$ = −0.89 V)26 to CH_2Cl_2 solutions of $[\mathbf{2}H]^+$ and $[\mathbf{3}H]^+$, cyclic voltammograms displayed increased cathodic current coinciding with the hydride reduction event indicative of proton reduction catalysis (Figure 9). At the relevant potentials (~ −1.5 V) proton reduction by the glassy carbon working electrode was confirmed to be negligible.26 In the case of $[\mathbf{4}H]^+$, addition of CF_3CO_2H resulted in the appearance of a new catalytic current ~200 mV milder than the $[\mathbf{4}H]^{+/0}$ couple (Figure 10). We attribute this new feature to catalysis by the *N*-protonated pyridine $[\mathbf{4}H_2]^{2+}$ complex, consistent with the previous spectroscopic results. Because $[\mathbf{4}H_2]^{2+}$ degrades into $[\mathbf{1}H]^+$ at

high concentrations of $CF3CO_2H$ (10-100 equiv), the voltammograms display an additional catalytic wave for $[\mathbf{1}H]^+$.

Plots of i_c/i_p (i_c = catalytic current, i_p = current in the absence of acid) vs $[CF_3CO_2H]$ are linear up to about i_c/i_p ~16-20 (Figure 11). This linear dependence indicates that H_2 evolution follows protonation of the reduced hydride, i.e. the rate is second order in $[H^+]$.27 The initial slope of this plot is a measure of the acid-dependent rate-determining step. For the hydrides investigated, this step is the protonation of Ni(I)Fe(I) precursors to form hydrides. Catalysis by the sterically more accessible catalyst, **1**, displays a steeper initial slope than the substituted derivatives **2** and **3** even though the latter are more basic. Relative to **2** and **3**, the greater steric accessibility of **1** toward protonation is consistent with the finding that $[\mathbf{1}H]^+$ is rapidly deprotonated by Et_3N whereas $[\mathbf{3}H]^+$ requires hours to deprotonate by the same strong base. The relative catalytic activity can be estimated from the acid-independent regions of the graph of i_c/i_p vs $[CF_3CO_2H]$.28 When the rate of catalysis in no longer dependent on $[H^+]$, the values for i_c/i_p = 16-20 indicate an acid-independent rate constant between 50-75 s^{-1}. For the tricarbonyl $[\mathbf{1}H]^+$, an i_c/i_p = 10 corresponds to an acid-independent rate constant of 20 s^{-1}.

To determine overpotential, electrocatalysis was conducted in MeCN solution, where the standard reduction potential of the acid to release H_2, $E^\circ_{HA/H2}$, can been determined.29 For CF_3CO_2H in MeCN solution, $E°$ is 0.89 V. Cyclic voltammetry of a freshly prepared MeCN solution of $[\mathbf{3}H]^+$ displayed the $[\mathbf{3}H]^{+/0}$ couple at −1.45 V, and the cathodic current dramatically increased upon addition of CF_3CO_2H. The overpotential is estimated at ~430 mV (Figure 9). For the pyridinium complex $[\mathbf{4}H_2]^{2+}$, overpotential is significantly smaller, ~260 mV (Figure 10).

Relevant to the mechanism of H_2 production is the finding that the reversibility of the $[\mathbf{2}H]^{+/0}$ couple is diminished in the presence of $[HNEt_3]BF_4$. This effect is consistent with the reduced derivative $[\mathbf{2}H]^0$ being sufficiently basic to undergo protonation by $[HNEt_3]^+$. Since $[HNEt_3]BF_4$ is unable to protonate **2**, the system **2**/$[HNEt_3]^+$ is catalytically inactive (in contrast to **2**/$[CF_3CO_2H]^+$). To further clarify the mechanism of hydrogen production, we found that in the presence excess acid, the catalytic current depends linearly on the concentration of $[\mathbf{3}H]^+$. Thus, the catalysis is first-order in $[\mathbf{3}H]^+$.

Acidity of Nickel-Iron Hydrides

To better understand the thermodynamic properties of the catalysts, we sought to determine both the pK_a of the new nickel-iron hydrides and the electrochemical properties of the resulting neutral NiFe compounds. Compounds **1** and **2** are poorly soluble in MeCN, a solvent with a well-established pK_a scale,30 We therefore employed PhCN as the solvent for the pK_a determinations. Although PhCN does not have an established pK_a scale, others have found that it behaves similarly to MeCN solutions.28 A dilute solution of $[\mathbf{1}H]^+$ in PhCN with one equivalent of aniline ($[PhNH_3]BF_4$ pK_a^{MeCN} = 10.7) afforded a stable 1:1 equilibrium mixture of $[\mathbf{1}H]^+$ and **1**, indicating a pK_a of ~10.7 for $[\mathbf{1}H]^+$. Similarly, four equiv of 4-methoxypyridine ([4-methoxypyridinium)]BF_4 pK_a^{MeCN} = 14.23)30 and $[\mathbf{3}H]^+$ provided an 2:1 equilibrium ratio of **3** and $[\mathbf{3}H]^+$, as determined by ^{31}P NMR spectroscopy. Although decomposition of the organometallic species occurred over several hours, we assign the pK_a as ~14.9 ± 0.1 as the **3**:$[\mathbf{3}H]^+$ ratio remained unchanged throughout the decomposition. For comparison with these results, the μ-hydrido diiron complex $[HFe_2(pdt)(CO)_4(PMe_3)_2]BF_4$ has pK_a^{MeCN} of 12.31

Using cyclic voltammetry, we determined the oxidation potentials **1** and **3**. Similar to the pK_a determination, PhCN was used to approximate $E_{1/2}$ values on the MeCN scale. A ~1

mM solution of **1** in PhCN displayed oxidation events, one reversible at −0.543 V and a second irreversible event at −0.124 V (Table 2). The cyclic voltammogram for **3** was similar, displaying a reversible oxidation at −0.722 V and an irreversible oxidation event at −0.191 V. We assign these couples as one-electron processes because the oxidation of **1** has been shown to afford the monocation.14

Discussion

The new hydride complexes are confirmed to be robust and functional models for the [NiFe]-hydrogenases, at least with respect to certain structural features and their ability to catalyze hydrogen evolution. Specifically, the hydrides represent structural mimics of the Ni-R form of these enzymes, an $S = 0$ state that is thought to feature an $Fe(\mu\text{-}SR)_2(\mu\text{-}H)Ni$ core.1 In the model complexes, the coordination sphere at Ni is square pyramidal, having rearranged from the tetrahedral geometry of the Fe(I)Ni(I) precursor. Such a rearrangement does not occur in the protein, wherein the Ni center adopts a geometry intermediate between square-planar and tetrahedral.4 Our DNMR studies also reveal a oscillatory motion that interchanges equivalent structures of the $Fe(CO)_2(PR_3)$ site. This dynamic equilibrium does *not* operate in the protein, as the interchange process would place a cyanide ligand in an apical site.

The present paper describes examples of hydride complexes that sustain at least quasi-reversible redox events. Reversible redox has been observed in a few bimetallic hydrides32 but is rare for monometallic hydrides where redox changes the pK_a by many orders of magnitude, which often precludes reversibility.33,34 Nature's selection of *bi*metallic active sites in the [FeFe]- and [NiFe]-hydrogenases thus provides a way to soften the effect of redox on the acid-base properties of the hydride. The pK_a and electrochemical data allow us to estimate the homolytic and heterolytic bond energies for the bond between the NiFe center and the μ-H ligand. Following the relations in eq 5 and 6, the free energies of H• donation, $\Delta G_{H\bullet}$, are calculated to be ~57 kcal/mol. These are relatively weak M-H bonds, 34,35 indicative of the stability of the mixed valence derivatives. Substitution of CO by PPh_3 affects the $[NiFe]^{I,I/I,II}$ and $[NiFe]^{I,II/II,II}$ couples as well as the pK_a. Comparing $[\mathbf{1}H]^+$ to $[\mathbf{3}H]^+$, the ΔpK_a of 4.2 corresponds to 5.7 kcal/mol. The $\Delta E_{1/2}$ of the $[HNiFe]^{+/0}$ couples corresponds to 4.6 kcal/mol. Consequently, although $[\mathbf{3}H]^+$ more difficult to reduce than $[\mathbf{1}H]^+$, its formation requires weaker acids and thus its catalytic function operates at a lower overpotential.

Although the $\mathbf{1}^{0/+}$ and $\mathbf{3}^{0/+}$ couples are reversible, the couples $\mathbf{1}^{+/2+}$ and $\mathbf{3}^{+/2+}$ are not. Both are required to calculate ΔG_{H^-}, the affinities of $[\mathbf{1}]^{2+}$ and $[\mathbf{3}]^{2+}$ for H^-. The ~0.5 V difference observed between the first and second potentials is expected,36 so these redox potentials were used to approximate the hydride donor strength for $[\mathbf{1}H]^+$ and $[\mathbf{3}H]^+$ (Table 2). These data suggest that the $[\mathbf{1}]^{2+}$ and $[\mathbf{3}]^{2+}$ have very high affinities for hydrides, the high positive charge and bimetallic structure being contributing factors.

$$\Delta G_{H\bullet} = 1.37 pK_a + 23.06 E_{1/2}^{I,I/I,II} + 54.9 \quad (5)$$

$$\Delta G_{H^-} = 1.37 pK_a + 23.06 E_{1/2}^{I,I/I,II} + 23.06 E_{1/2}^{I,II/II,II} + 79.6 \quad (6)$$

One of the more striking results is the asymmetry of the Fe-H-Ni linkage, which is probably relevant to the mechanism by which these complexes reduce protons. In the parent hydride $[HNiFe(pdt)(dppe)(CO)_3]BF_4$, ($[\mathbf{1}H]BF_4$) the difference of the iron-hydride and nickel-

hydride bond distances (*Δd*(M-H)) is 0.15 Å, whereas in [HNiFe(pdt)(dppe)(PPh_3)($CO)_2$]BF_4, the Ni-H bond is 0.4 Å longer than the Fe-H bond (Table 3). Although terminal hydrides are invoked for the catalytic mechanism of [FeFe]-hydrogenases, catalytically active μ-hydrido diiron dithiolates have been reported.6 Such μ-hydride catalysts are mechanistically and structurally more closely related to the [NiFe]-hydrogenases.13 The high asymmetry of the Ni-H-Fe linkage in the present cases suggests that even in the [NiFe] enzymes, the Fe-H bond may have significant character as a terminal (vs bridging) hydride.

Catalysis by these complexes operates via the sequence of reactions in Scheme 3. The voltammetric responses indicate that the reaction is second order in protons and first order in the bimetallic complex. The rate of proton depends on both the basicity of the metal center and steric effects.41 The associated acid-dependent rate constants are not effective benchmarks for catalytic efficiency, in part because they depend on the proton source.42 More useful are the relative rates for catalysis in the acid-independent regime obtained at high [H^+], as well as the overpotential (Table 3).43 This high [H^+] regime resembles enzymatic conditions where protons are efficiently provided to the NiFe center.44 In this [H^+] regime, the rate-limiting step is assumed to be the dissociation of H_2 from the doubly protonated catalyst.6

Pyridylphosphines confer fascinating properties to certain catalysts48 and offered the possibility of facilitating proton transfer.49 When installed on diiron dithiolates, pyridyl phosphines undergo *N*-protonation, which leads to milder E_{cat}, an effect attributable to an electrostatic influence.50 We observe similar effects in this study: the overpotential decreases by ~140 mV for the dication [**4**H_2]$^{2+}$ vs [**4**H]$^+$ (Table 3). The amine also accelerates the deprotonation of the μ-hydride, which is otherwise slow. The pathway by which this deprotonation occurs is suggested by the observation that the hydride exists in equilibrium with the pyridinium salt. In the protein, the protons exchange between the metal centers (hydride ligands) and the terminal thiolate ligands.4

Experimental

Unless otherwise indicated, reactions were conducted using Schlenk and cannula-filtration techniques at reduced temperatures. Solvents for syntheses were HPLC-grade and further purified using an alumina filtration system (Glasscontour Co., Irvine, CA), NMR solvents were either dried with CaH_2 and stored under nitrogen over activated 3 Å molecular sieves or purchased as ampoules from Cambridge Isotope Laboratories. Diiron nonacarbonyl, tetrafluoroboric acid in diethyl ether, triphenylphosphite, triphenyphosphine, and trifluoroacetic acid were purchased from Aldrich and used as received. Tetrabutylammonium hexafluorophosphate (Aldrich) was recrystallized from methylene chloride and hexane. NMR spectra were recorded at room temperature on a Varian Mercury spectrometer. NMR chemical shifts are quoted in ppm; spectra are referenced to TMS for ^{1}H and 85% H_3PO_4 for $^{31}P\{^1H\}$ spectra.

NiFe(pdt)(dppe)$(CO)_3$, 1

To a 500-mL round bottomed Schlenk flask with stir bar was added 2.25 g (4.01 mmol) of Ni(pdt)(dppe), 1.52 g (4.19 mmol) of $Fe_2(CO)_9$, and 40 mL of CH_2Cl_2. After stirring the red slurry for 6 h, solvent was removed under vacuum, and the red residue was washed with four 30 mL portions of MeCN to remove Fe_2(pdt)$(CO)_6$ and $Fe(CO)_5$. The remaining red-green solid was extracted into ca. 5 mL of CH_2Cl_2, and this extract was filtered through 4 × 12 cm plug of silica gel, rinsing with CH_2Cl_2. A mobile green product eluted, leaving unreacted Ni(pdt)(dppe). The green solution was then concentrated and then diluted with 100 mL of hexane to precipitate green microcrystals. Yield: 0.745 g (1.06 mmol, 27%). ^{1}H NMR (500 MHz, CD_2Cl_2, 20 °C): δ 1.3 (1H, *qt*, axial $(SCH_2)_2CH_2$), 1.85 (1H, *dt*, equatorial

($SCH_2)_2CH_2$), 1.9 (2H, *t*, axial ($SCH_2)_2CH_2$), 2.5 (2H, *dt*, equatorial ($SCH_2)_2CH_2$), 2.2 (4H, m, PCH_2CH_2P), 7.4 - 7.7 (20H, *m*, C_6H_5). $^{31}P\{^1H\}$ NMR (202 MHz, CD_2Cl_2): δ 63.6. FT-IR (CH_2Cl_2): ν_{CO} = 2028, 1952 cm^{-1}.

[HNiFe(pdt)(dppe)(CO)$_3$]BF$_4$, [1H]BF$_4$

To a 100-mL round bottomed Schlenk flask with magnetic stir bar was added 1.25 g (1.78 mmol) of **1** and 10 mL of CH_2Cl_2. To this green solution was added 0.30 mL (2.078 mmol) of HBF_4•Et_2O, immediately producing a red solution. The solution was then concentrated under vacuum and the product was precipitated by the addition of ~20 mL of Et_2O. Recrystallization from CH_2Cl_2/Et_2O afforded red microcrystals. Yield: 1.35 g (1.71 mmol, 96%). ^1H NMR (500 MHz, CD_2Cl_2, 20 °C): δ −3.53 (1H, *tt*: J_{PH} = 6, J_{HH} = 0.6 Hz correlates with signal at δ2.5, *H*NiFe), 1.57 (1H, *qt*, axial ($SCH_2)_2CH_2$), 2.0 (2H, *t*, axial ($SCH_2)_2CH_2$), 2.5 (2H, *d*, equatorial ($SCH_2)_2CH_2$), 2.65 (1H, *dt*, equatorial ($SCH_2)_2CH_2$), 2.78 (4H, *m*, PCH_2CH_2P), 7.5 - 8.0 (20H, m, C_6H_5). ^{31}P NMR (202 MHz, CD_2Cl_2): δ 71. $^{13}C\{^1H\}$ NMR (19 °C, CD_2Cl_2, 150 MHz): δ 26, 36 (s, 2:1, pdt CH_2); 30 (*t*, $^1J_{PC}{\sim}^2J_{PC}$ = 10 Hz, PCH_2CH_2P); 130, 134, 134.5 (PPh_n); 204 (s, Fe($CO)_3$), 205 (s, Fe($CO)_3$). FT-IR (CH_2Cl_2): ν_{CO} = 2082, 2024 cm^{-1}. Anal. Calcd for $C_{32}H_{31}BF_4FeNiO_3P_2S_2$ (found): C, 50.10 (50.16); H, 4.55 (4.75). Single crystals of [**1**H]BF_4·CH_2Cl_2 were grown from CH_2Cl_2-ether.

Reaction of 1 with B(C$_6$F$_5$)$_3$ and H$_2$

Under an inert atmosphere 4.0 mg $B(C_6F_5)_3$ (0.0078 mmol) and 6.6 mg (0.0094 mmol) of **1** was dissolved with ~0.5 mL CD_2Cl_2 in a J. Young NMR tube. The ^1H and $^{31}P\{^1H\}$ NMR spectra were recorded initially showing ~16% conversion to the hydride [**1**H]$^+$, which we attribute to the action of $(H_2O)B(C_6F_5)_3$. Spectra recorded after 1 h verified that no change occurred. The sample was then frozen and put under an H_2 atmosphere. ^1H and $^{31}P\{^1H\}$ NMR spectra showed nearly complete conversion to [**1**H]$^+$.

[HNiFe(pdt)(dppe)(P(OPh)$_3$)(CO)$_2$]BF$_4$, [2H]BF$_4$

To a 250-mL round bottomed Schlenk flask was dissolved 1.245 g (1.58 mmol) of [**2**H]BF_4 in 40 mL of CH_2Cl_2. To this solution, 414 μL (1.58 mmol) of $P(OPh)_3$ was added and the mixture was stirred for 6 h at 35 °C. Solvent was then removed under vacuum, and the product was extracted into a small amount of warm EtOH. Cooling of this extract to −78 °C precipitated the red product. This process was repeated 3× followed by recrystallization of the material from an EtOH solution by the addition of hexane. Yield: 1.06 g (1.0 mmol, 62%). ^1H NMR (400 MHz, CD_2Cl_2): δ 6.6-8.0 (35H, *m*, Ph's), 2.88-1.1 (PCH_2CH_2P, $SCH_2CH_2CH_2S$), −3.45 (1H, *dt*, Ni(μ-H)Fe). $^{31}P\{^1H\}$ NMR (161 MHz, CD_2Cl_2): δ 161 (*s*, $P(OPh)_3$), 65.8 (*br*, dppe). FT-IR (CH_2Cl_2): ν_{CO} = 2031, 1981 cm^{-1}.

[HNiFe(pdt)(dppe)(PPh$_3$)(CO)$_2$]BF$_4$, [3H]BF$_4$

Method A—To a 100-mL round bottomed Schlenk flask fitted with magnetic stir bar was added 0.126 g (0.180 mmol) of NiFe(pdt)(dppe)$(CO)_3$ from the glove-box and dissolved in 25 mL of CH_2Cl_2. To this green solution 0.077 g of (0.220 mmol) [$HPPh_3$]BF_4 and 0.105 g (0.400 mmol) of PPh_3 were added. After 3.5 h photolysis with a Spectroline black light lamp (365 nm), the FT-IR spectrum showed complete consumption of [**1**H]BF_4. The solution was then concentrated under vacuum and addition of 40 mL of Et_2O provided a red precipitate. The product was washed with 3 × 10 mL of Et_2O, and dried under vacuum. Yield: 0.113 g (0.121 mmol, 67%).

Method B—To a 250-mL round bottomed flask fitted with magnetic stir bar was prepared a solution of 0.262 g (0.333 mmol) of [**1**H]BF_4 in 50 mL of THF. To this solution 0.98 g

(3.74 mmol, ~10×) of PPh_3 was added. After stirring the solution for 2 h at 40 °C, the solvent was removed in vacuum yielding an red colored oil, which was washed with four 20-mL portions of hexane. The remaining oil was redissolved in 30 mL of CH_2Cl_2, and the microcrystalline product was precipitated by addition of 100 mL of hexane. Yield: 0.235 g (0.230 mmol, 70%). ^{1}H NMR (400 MHz, CD_2Cl_2): δ 6.8-7.9 (35H, *m*, C_6H_5), $\tilde{8}_7$ (4H, *m*, PCH_2CH_2P), 2.7-1.4 (6H, *m*, $SCH_2CH_2CH_2S$), δ −3.08 (1H, *dt*, Ni(μ-H)Fe). $^{31}P\{^1H\}$ NMR (161 MHz, CD_2Cl_2): δ 69.5 (*s*, PPh_3), 65.8 (*br*, dppe). $^{13}C\{^1H\}$ NMR (19 °C, CD_2Cl_2, 150 MHz): δ 25.0, 25.75, 36.2 (s, 1:1:1, pdt CH_2's); 28.6 (br, PCH_2CH_2P); 128-134 (m br, PPh_n); 211 (br, $Fe(CO)_2$). $^{13}C\{^1H\}$ NMR (−60 °C, CD_2Cl_2, 150 MHz): δ 24.95, 25.56, 36.62 (pdt CH_2's), 27.98 + 29.18 (br, dppe PCH_2CH_2P), 128-134 (m br, C_6H_5), 211.2 + 211.6 (br, $Fe(CO)_2$). FT-IR (CH_2Cl_2): ν_{CO} = 2016, 1964 cm^{-1}. Anal. Calcd for $C_{49}H_{46}BF_4FeNiO_2P_3S_2$ (found): C, 57.40 (57.48); H, 4.52 (4.36).

NiFe(pdt)(dppe)(PPh_3)$(CO)_2$, 3

In a 100-mL round-bottomed Schlenk flask was dissolved 0.110 g (0.107 mmol) of [**3**H]BF_4 in 5 mL of CH_2Cl_2 and 2 mL of MeOH. To this red solution 5.8 mg (0.107 mmol) of NaOMe was added. After stirring for 3 h, the reaction mixture was evaporated under vacuum. The residue was washed with H_2O (3 × 5 mL) and MeOH (3 × 5 mL), and the green powder was dried under vacuum. Yield: 74 mg (0.079 mmol, 74%). ^{1}H NMR (400 MHz, CD_2Cl_2): δ 7.2-8.0 (35H, *m*, C_6H_5), $\tilde{8}_I$ (4H, *m*, PCH_2CH_2P), 1.8-0.8 (6H, *m*, $SCH_2CH_2CH_2S$). $^{31}P\{^1H\}$ NMR (161 MHz, CD_2Cl_2): δ 55 (*t*, PPh_3), 45 + 77 (*br*, dppe). FT-IR (CH_2Cl_2): ν_{CO} 1971, 1916 cm^{-1}. Anal. Calcd for $C_{49}H_{45}FeNiO_2P_3S_2$ (found): C, 62.10 (62.78); H, 4.78 (4.45).

[HNiFe(pdt)(dppe)(PPh_2Py)$(CO)_2$]BF_4 ([4H]BF_4) and its Protonation

To a 250-mL round bottom Schlenk flask was added 0.400 g [**1**H]BF_4 (0.508 mmol) and dissolved in 30 mL THF. To this solution 0.150 g (0.570 mmol, ~1.1×) of Ph_2PyP was added. After stirring the solution for 3 h at 40 °C, solvent was concentrated and the product was precipitated by addition of Et_2O. The red solid was recrystallized from 15 mL of acetone by the addition of 60 mL of EtOAc. The red microcrystalline material was dried under vacuum and stored in the glovebox. Yield: 0.309 g (0.302 mmol, 59%). ^{1}H NMR (500 MHz, CD_2Cl_2): δ 6.8-7.9, 8.8 (35H, *m*, C_6H_5, C_5H_4N), $\dot{\delta}\tilde{8}_{62}$ (4H, *m*, PCH_2CH_2P), δ 2.53-1.49 (6H, *m*, $SCH_2CH_2CH_2S$), $\tilde{\delta}_{3.19}$ (1H, *dt*, Ni(μ-H)Fe). $^{31}P\{^1H\}$ NMR (202 MHz, CD_2Cl_2): δ 73.7 (*s*, PPh_2Py), 65.7 (*br*, dppe). FT-IR (CH_2Cl_2): ν_{CO} = 2022, 1971 cm^{-1}. Samples of [**4**H_2]$^{2+}$ were generated by protonation of degassed CH_2Cl_2 solutions with ~5 equiv of CF_3CO_2H, however the resulting dication was observed to decompose over the course of minutes. The decomposition mixture consisted of [**1**H]BF_4, Ni(pdt)(dppe), and [$HPPh_2Py$]$^+$ as indicated by $^{31}P\{^1H\}$ and ^{1}H NMR spectra. ^{1}H NMR (400 MHz, CD_2Cl_2): δ 7.2-7.8 (*m*), 8.0 (*t*), 8.3 (*t*), 8.8 (*d*) (35H, C_6H_5, C_5H_4N), $\dot{\delta}\tilde{8}_6$ (4H, *m*, PCH_2CH_2P), δ 2.7-1.5 (6H, *m*, $SCH_2CH_2CH_2S$), $\tilde{8}_{14}$ (1H, *dt*, Ni(μ-H)Fe). $^{31}P\{^1H\}$ NMR (161 MHz, CD_2Cl_2): δ 79 (*s*, PPh_2Py), 66 (*br*, dppe). FT-IR (CH_2Cl_2): ν_{CO} = 2032, 1982 cm^{-1}.

pK_a Determination of [3H]BF4

In a J. Young NMR tube, ~0.8 mL dry degassed PhCN was added to 10.0 mg (0.0098 mmol) of [**3**H]BF_4. To this solution 197 μL of a freshly prepared solution of 0.197 M of 4-methoxypyridine in PhCN (pK_a^{MeCN} = 14.23) was added. The ^{31}P NMR spectrum was then recorded after 1, 2, 3, and 5 h. At each interval the ratio of **3**:[**3**H]$^+$ remained unchanged at 2:1, despite steady decomposition of the sample. The ratio was determined by integration of the respective PPh_3 signals.

pK_a Determination of [1H]BF_4

In a 25 mL Schlenk flask, ~4 mL dry degassed PhCN was added to 5.8 mg (0.0073 mmol) of [**1**H]BF_4. To this solution 27.6 μL of a freshly prepared solution of 0.5 M of aniline in PhCN (pK_a^{MeCN} = 10.7)25 was added. The FT-IR spectrum was then recorded after 3, 8, and 18 h. At each interval the ratio of **1**:[**1**H]$^+$ remained unchanged at 1:1.

H/D Exchange of [3H]BF_4 with D_2O

Under an inert atmosphere 4.3 mg (0.0042 mmol) of [**3**H]BF_4 was dissolved with ~0.5 mL d^6-acetone (ampoule, Cambridge) in a J. Young NMR tube. A ^{1}H NMR spectrum was recorded for t = 0, then 10 μL (0.56 mmol) D_2O was added (in air) and subsequent scans were collected by at ~2 min intervals. The intensity of the μ-H signal (δ −3.08), determined vs phenyl region, decayed in a first order manner. After the complete disappearance of the hydride signal for [**3**H]BF_4, a ^{31}P{^{1}H} spectrum was recorded, verifying the presence of the deuteride ([**3**D]BF_4) with no decomposition.

H/D Exchange of [4H]BF_4 with D_2O

A solution of 7.2 mg (0.00705 mmol) of [**4**H]BF_4 in ~0.5 mL d^6-acetone was prepared in a J.Young NMR tube. The ^{1}H NMR spectrum was recorded for t = 0. The sample was then frozen, 10 μL (0.56 mmol) D_2O was added, and the sample tube evacuated and then thawed. A ^{1}H NMR spectrum was recorded ~5 min after thawing, showing nearly complete consumption of the hydride signal (δ −3.19). A ^{31}P{^{1}H} spectrum verified the presence of the deuteride complex ([**4**D]BF_4) with no decomposition.

Kinetics of Deprotonation of [3H]BF_4 with NEt_3

In a J.Young NMR tube, a solution of 5.4 mg (0.0052 mmol) of [**3**H]BF_4 in ~0.5 mL CD_2Cl_2 was treated with 12 μL (0.086 mmol) of NEt_3 added by syringe. The tube was then sealed, and ^{1}H and ^{31}P{^{1}H} NMR spectra were recorded. The first-order decay plot was constructed from ^{31}P{^{1}H} NMR spectra, as the ratio of **3**/[**3**H]BF_4 could be readily determined by integration of the respective PPh_3 signals. The ^{1}H NMR data confirm the pseudo-first order behavior.

Electrochemistry, General Considerations

As the nickel-iron hydrides presented in this paper degrade over the course of minutes in MeCN solution, electrochemistry was mainly performed on CH_2Cl_2 solutions. Cyclic voltammetry experiments were carried out in a 20-mL one compartment glass cell with tight-fitting Teflon lid with three tight-fitting electrodes and nitrogen gas inlet, interfaced with a BAS-100 Electrochemical Analyzer. The working electrode was a glassy carbon disk (diameter: 0.3 cm). A silver wire was used as a pseudo-reference electrode, and the counter electrode was a Pt wire. The electrolyte was 0.1 M Bu_4NPF_6 in CH_2Cl_2. Ferrocene was added as an internal reference and cyclic voltammograms were each referenced to this $Fc^{0/+}$ couple (0.00 V). *i*R compensation was applied: solutions were pulsed prior to each scan to determine the cell resistance, this compensation was applied to the subsequent voltammogram. Between scans electrodes were polishing with alumina.

Overpotentials are estimated from the potential at 0.5(i_{pc}) where i_{pc} is the peak current in the acid-independent regime (see Figure 11). Using the acidity constant for CF_3CO_2H (TFA) in MeCN solution, pK_{TFA}^{MeCN}, of 12.65 (and ignoring homoconjugation),25 $E°_{TFA/H2}$ was calculated using Evans' relationship (eq 5).26

$$E^\circ_{\mathrm{TFA}} = E^\circ_{H+} - (2.303RT/F)\,\mathrm{p}K_{TFA}{}^{MeCN} = -0.89\ \mathrm{V} \quad (5)$$

Cyclic Voltammetry for [2H]BF_4 and 2

A solution of 2.6 mg (0.00243 mmol) of [**2**H]BF_4 in 5 mL of CH_2Cl_2 was prepared in the CV cell and was treated with successive aliquots (18 μL, 2 equiv) of freshly prepared 0.268 M CF_3CO_2H-CH_2Cl_2 solution. Cyclic voltammograms were recorded at 100 mV/s. A solution of 14.0 mg (0.013 mmol) of [**2**H]BF_4 in 5 mL of CH_2Cl_2 was prepared in the CV cell, and cyclic voltammograms were recorded at various scan rates. The solution was then treated with 10 μL of NEt_3, 5 8g (0.045 mmol) of KO^{t}Bu, and 2 drops of MeOH, then stirred for 1 h prior to recording voltammograms for [**2**]$^{0/+}$. Studies on [**3**H]BF_4 (3.3 mg in 5 mL CH_2Cl_2) and [**3**H]BF_4 (4.9 mg in 5 mL) were conducted similarly.

Cyclic Voltammetry for [4H]BF_4

A solution of 3.8 mg (0.0037 mmol) of [4H]BF4 in 5 mL of CH_2Cl_2 was prepared in the CV cell and was treated with successive aliquots (27.7 μL, 2 equiv) of a freshly prepared solution of 0.268 M CF_3CO_2H in CH_2Cl_2 solution. Cyclic voltammograms were recorded at 100 mV/s. To determination the order with respect to [**4**H]BF_4, a solution of 145 μL of CF_3CO_2H in 5 mL of CH_2Cl_2 was prepared in the CV cell and treated with successive amounts of solid [**4**H]BF_4. The result of this titration assigns catalysis as first-order with respect to [**4**H]BF_4.

Supplementary Material

Refer to Web version on PubMed Central for supplementary material.

Acknowledgments

This research was sponsored by NIH. We thank Dr. Danielle Gray for the crystallographic analysis of [**3**H]BF_4.

References

(1). De Lacey AL, Fernández VM, Rousset M, Cammack R. Chem. Rev. 2007; 107:4304–4330. [PubMed: 17715982]

(2). Ogata H, Lubitz W, Higuchi Y. Dalton Trans. 2009; 7577:7587.

(3). Fontecilla-Camps JC, Amara P, Cavazza C, Nicolet Y, Volbeda A. Nature. 2009; 460:814–822. [PubMed: 19675641]

(4). Fontecilla-Camps JC, Volbeda A, Cavazza C, Nicolet Y. Chem. Rev. 2007; 107:4273–4303. [PubMed: 17850165]

(5). Heinekey DM. J. Organometal. Chem. 2009; 694:2671–2680.

(6). Gloaguen F, Rauchfuss TB. Chem. Soc. Rev. 2009; 38:100–108. [PubMed: 19088969]

(7). Reihlen H, von Friedolsheim A, Ostwald W. Justus Liebigs Ann. Chem. 1928; 465:72–96.Hieber W, Spacu P. Z. anorg. allgem. Chem. 1937; 233:852–864.King RB. J. Am. Chem. Soc. 1962; 84:2460.Fauvel K, Mathieu R, Poilblanc R. Inorg. Chem. 1976; 15:976–978.Winter A, Zsolnai L, Huttner G. Z. Naturforsch. 1982; 37b:1430–1436.

(8). Cammack, R.; Frey, M.; Robson, R. Hydrogen as a Fuel: Learning from Nature. Taylor & Francis; London: 2001.

(9). Ludwig M, Cracknell JA, Vincent KA, Armstrong FA, Lenz O. J. Biol. Chem. 2009; 284:465–477. [PubMed: 18990688]

(10). Vincent KA, Parkin A, Armstrong FA. Chem. Rev. 2007; 107:4366–4413. [PubMed: 17845060]

(11). Tard C, Pickett CJ. Chem. Rev. 2009; 109:2245–2274. [PubMed: 19438209] van der Vlugt JI, Meyer F. Met. Ions Life Sci. 2007; 2:181–239.

(12). Li Z, Ohki Y, Tatsumi K. J. Am. Chem. Soc. 2005; 127:8950–8951. [PubMed: 15969562] Ohki Y, Yasumura K, Kuge K, Tanino S, Ando M, Li Z, Tatsumi K. Proc. Natl. Acad. Sci. U.S.A. 2008; 105:7652–7657. [PubMed: 18511566] Pal S, Ohki Y, Yoshikawa T, Kuge K, Tatsumi K. Chem. Asian J. 2009; 4:961–968. [PubMed: 19130447]

(13). Mealli C, Rauchfuss TB. Angew. Chem. Int. Ed. 2007; 46:8942–8944.

(14). Barton BE, Whaley CM, Rauchfuss TB, Gray DL. J. Am. Chem. Soc. 2009; 132:6942–6943. [PubMed: 19413314]

(15). Whaley CM, Rauchfuss TB, Wilson SR. Inorg. Chem. 2009; 48:4462–4469. [PubMed: 19374433]

(16). van der Vlugt JI, Rauchfuss TB, Whaley CM, Wilson SR. J. Am. Chem. Soc. 2005; 127:16012–16013. [PubMed: 16287273]

(17). Koper MTM, Bouwman E. Angew. Chem. Int. Ed. 2010; 49:3723–3725.

(18). Lai C-H, Reibenspies JH, Darensbourg MY. Angew. Chem., Int. Ed. Engl. 1996; 35:2390–2393.Verhagen JAW, Lutz M, Spek AL, Bouwman E. Eur. J. Inorg. Chem. 2003; 2003:3968–3974.

(19). Zhu W, Marr AC, Wang Q, Neese F, Spencer DJE, Blake AJ, Cooke PA, Wilson C, Schröder M. Proc. Natl. Acad. Sci. 2005; 102:18280–18285. [PubMed: 16352727]

(20). Schunn RA. Inorg. Chem. 1970; 9:394–395.

(21). Stephan DW. Dalton Trans. 2009:3129–3136. [PubMed: 19421613] Heiden ZM, Zampella G, De Gioia L, Rauchfuss TB. Angew. Chem., Int. Ed. 2008; 47:9756–9759.

(22). Justice, AK.; Zampella, G.; De Gioia, L.; Rauchfuss, TB.; van der Vlugt, JI.; Wilson, SR. Inorg. Chem. Vol. 46. 2007. p. 1655-1664.Justice, AK. Ph.D. Thesis. University of Illinois at Urbana-Champaign; 2008.

(23). Braterman, PS. Metal Carbonyl Spectra. Academic Press; London: 1975.

(24). Schilter, D.; Rauchfuss, TB. unpublished results

(25). Izutsu, K. Acid-Base Dissociation Constants in Dipolar Aprotic Solvents. Blackwell Scientific Publications; Oxford, U.K.: 1990.

(26). Felton GAN, Glass RS, Lichtenberger DL, Evans DH. Inorg. Chem. 2006; 45:9181–9184. [PubMed: 17083215]

(27). Wilson AD, Newell RH, McNevin MJ, Muckerman JT, DuBois M. Rakowski, DuBois DL. J. Am. Chem. Soc. 2006; 128:358–366. [PubMed: 16390166]

(28). Fraze K, Wilson AD, Appel AM, DuBois M. Rakowski, DuBois DL. Organometallics. 2007; 26:3918–3924.

(29). Wayner DDM, Parker VD. Accts. Chem. Res. 2002; 26:287–294.

(30). Kaljurand I, Kütt A, Sooväli L, Rodima T, Mäemets V, Leito I, Koppel IA. J. Org. Chem. 2005; 70:1019–1028. [PubMed: 15675863]

(31). Eilers G, Schwartz L, Stein M, Zampella G, de Gioia L, Ott S, Lomoth R. Chem.Eur. J. 2007; 13:7075–7084.

(32). Barton BE, Rauchfuss TB. Inorg. Chem. 2008; 47:2261–2263. [PubMed: 18333613]

(33). Tilset M. J. Am. Chem. Soc. 1992; 114:2740–2741.Cheng T-Y, Szalda DJ, Zhang J, Bullock RM. Inorg. Chem. 2006; 45:4712–4720. [PubMed: 16749835] Hamon P, Toupet L, Hamon J-R, Lapinte C. Organometallics. 1992; 11:1429–1431.

(34). Tilset, M. Comprehensive Organometallic Chemistry III. Crabtree, RH.; Mingos, DMP., editors. Elsevier; Oxford: 2007. p. 279-305.

(35). Choi J, Pulling ME, Smith DM, Norton JR. J. Am. Chem. Soc. 2008; 130:4250–4252. [PubMed: 18335937]

(36). Houser EJ, Venturelli A, Rauchfuss TB, Wilson SR. Inorg. Chem. 1995; 34:6402.

(37). Ezzaher S, Capon J-F, Gloaguen F, Pétillon FY, Schollhammer P, Talarmin J, Pichon R, Kervarec N. Inorg. Chem. 2007; 46:3426–3428. [PubMed: 17397148]

(38). Morvan D, Capon J-F, Gloaguen F, Le Goff A, Marchivie M, Michaud F, Schollhammer P, Talarmin J, Yaouanc J-J. Organometallics. 2007; 26:2042–2052.

(39). Zhao X, Hsiao Y-M, Lai C-H, Reibenspies JH, Darensbourg MY. Inorg. Chem. 2002:699–708. [PubMed: 11849069]

(40). Gloaguen F, Lawrence JD, Rauchfuss TB, Bénard M, Rohmer M-M. Inorg. Chem. 2002; 41:6573–6582. [PubMed: 12470052]

(41). Kramarz KW, Norton JR. Prog. Inorg. Chem. 1994; 42:1–65.

(42). Ezzaher S, Capon J-F, Dumontet N, Gloaguen F, Pétillon FY, Schollhammer P, Talarmin J. J. Electroanal. Chem. 2009; 626:161–170.

(43). Dubois, M. Rakowski; Dubois, DL. Acct. Chem. Res. 2009; 42:1974–1982.

(44). Gálvan IF, Volbeda A, Fontecilla-Camps JC, Field MJ. Proteins: Struct., Funct., Bioinf. 2008; 73:195–203.

(45). Pershad HR, Duff JLC, Heering HA, Duin EC, Albracht SPJ, Armstrong FA. Biochemistry. 1999; 38:8992–8999. [PubMed: 10413472]

(46). Connelly NG, Geiger WE. Chem. Rev. 1996; 96:877–922. [PubMed: 11848774]

(47). Leger C, Jones AK, Roseboom W, Albracht SPJ, Armstrong FA. Biochemistry. 2002; 41:15736–15746. [PubMed: 12501202]

(48). Hartwig, JF. Organotransition Metal Chemistry, from Bonding to Catalysis. University Science Books; New York: 2010. Drent E, Arnoldy P, Budzelaar PHM. J. Organomet. Chem. 1994; 475:57–63.

(49). DuBois, M. Rakowski; DuBois, DL. Chem. Soc. Rev. 2009; 38:62–72. [PubMed: 19088965] Barton BE, Olsen MT, Rauchfuss TB. J. Am. Chem. Soc. 2008; 130:16834–16835. [PubMed: 19053433] Grotjahn DB. Chem. Eur. J. 2005; 11:7146–7153.Grotjahn DB. Pure Appl. Chem. 2010; 82:635–647.

(50). Li P, Wang M, Chen L, Liu J, Zhao Z, Sun L. Dalton Trans. 2009:1919–1926. [PubMed: 19259561]

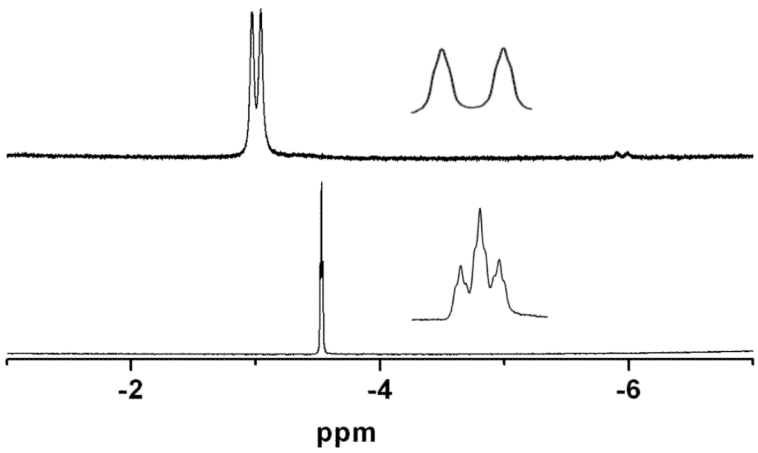

Figure 1.
500 MHz ^{1}H NMR spectra (CD_2Cl_2 solution) of [**1**H]BF_4 (bottom, triplet, J_{PH} = 6 Hz) and of [**3**H]BF_4 (top, doublet of triplets, J_{PH} = 35 Hz).

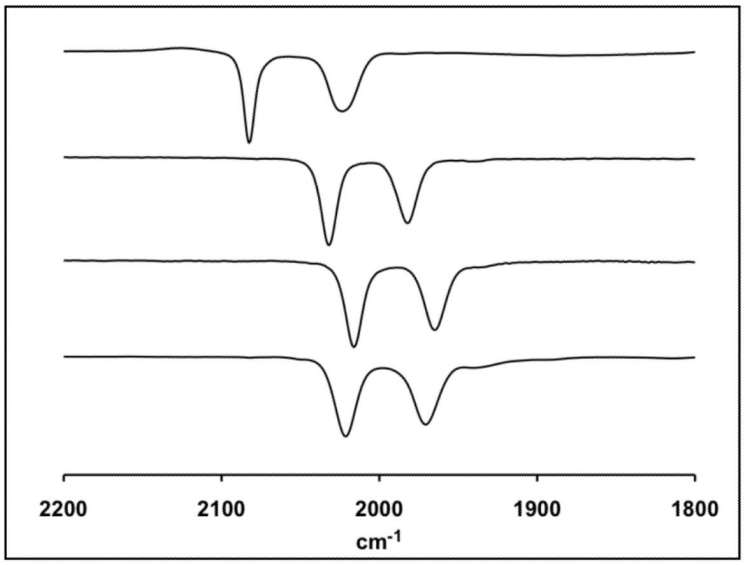

Figure 2.
FT-IR spectra in the ν_{CO} region for CH_2Cl_2 solutions of the nickel-iron hydride complexes described in this work (top to bottom): [**1**H]BF_4; [**2**H]BF_4; [**3**H]BF_4; [**4**H]BF_4. The ν_{CO} band for the Ni-R state occurs at 1936-1948 cm^{-1}, depending on the organism.1

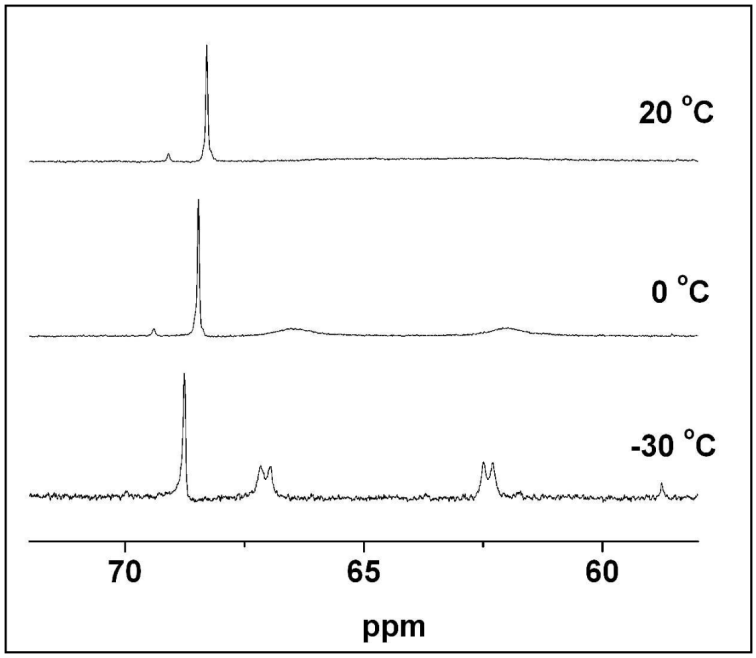

Figure 3.

$^{31}P\{^{1}H\}$ NMR (161 MHz) spectra of CD_2Cl_2 solutions of [**3**H]BF_4 recorded at various temperatures. The signal at δ 68 is assigned to the Fe(PPh_3) center. The dynamic AB quartet at δ 65 is assigned to the Ni(dppe) center. Weak signals at δ 59 and 69 were verified to arise from trace impurities of Ni(pdt)(dppe) and $[HNiFe(pdt)(dppe)(CO)_3]^+$, respectively.

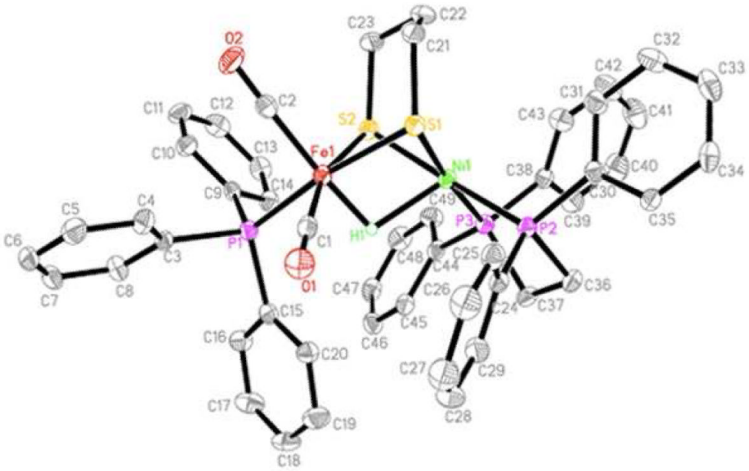

Figure 4.

Structure of [**3**H]BF_4. Selected distances (Å): Fe(1)-Ni(1), 2.6432(7); Fe(1)-H(1), 1.49(3); Ni(1)-H(1), 1.89(3). Selected Bond angles (°): S(2)-Fe(1)-S(1), 83.27(4); S(2)-Fe(1)-P(1), 93.58(4); C(1)-Fe(1)-C(2), 99.93(17).

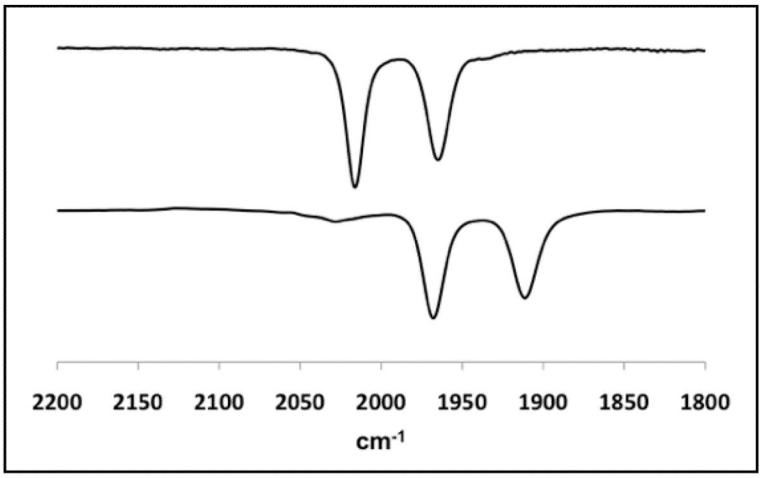

Figure 5.
FT-IR spectra of CH_2Cl_2 solutions of [**3**H]BF_4 (top) and **3** (bottom).

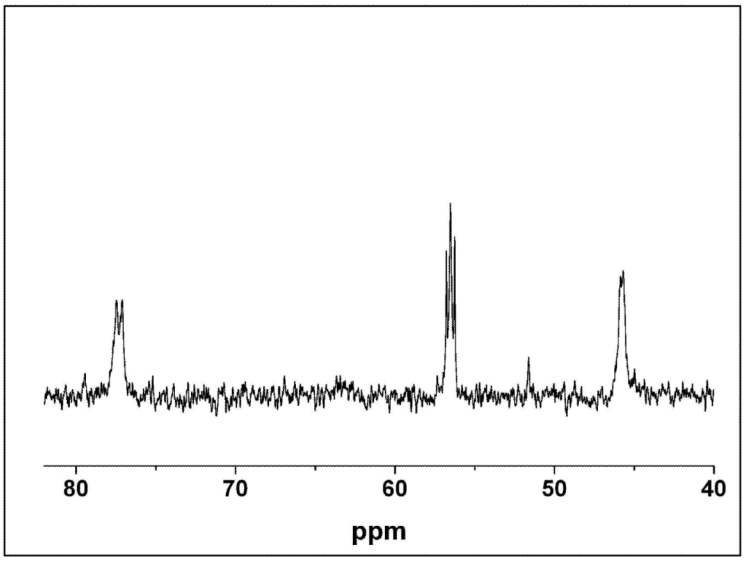

Figure 6.
$^{31}P\{^{1}H\}$ NMR spectrum (161 MHz, CD_2Cl_2, ~20 °C) of **3**. Signals at δ 77 and 45 are assigned to dppe, the signal at δ 55 is assigned to PPh_3.

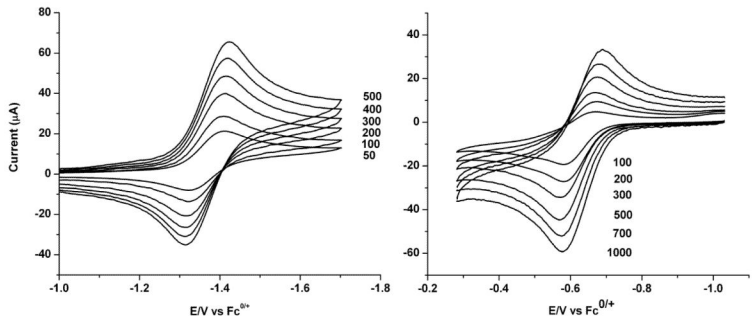

Figure 7.

Cyclic voltammograms of a 1.85 mM MeCN solution of $[\mathbf{2}H]^+$ (left) and a 1.68 mM 9:1 MeCN/CH_2Cl_2 solution (0.1 M $[NBu_4]PF_6$) of **2** (right) at various scan rates, denoted in mV/s.

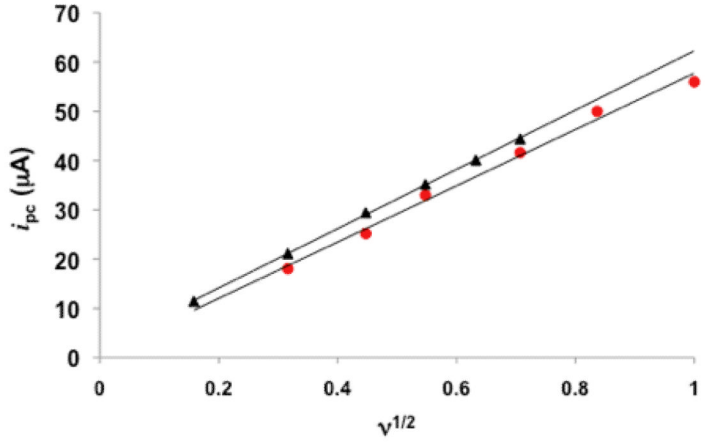

Figure 8.
Scan rate dependence of i_{pc} for the couples $[\mathbf{2}H]^{+/0}$ and $\mathbf{2}^{0/+}$ in CH_2Cl_2 solution (~1.8 mM complex, 0.1 M $[NBu_4]PF_6$).

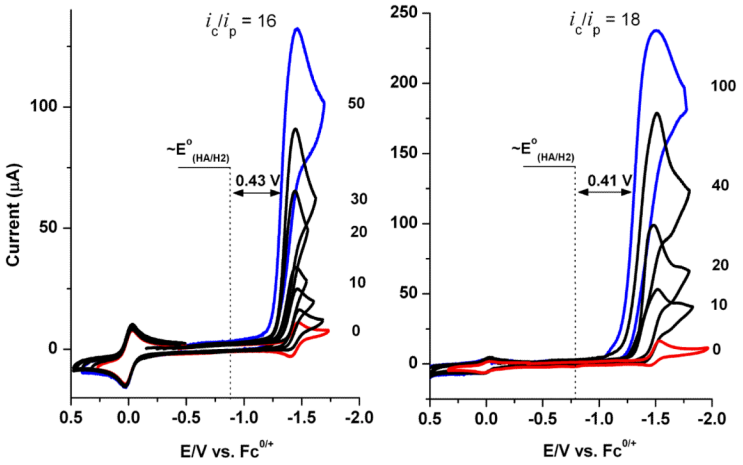

Figure 9.

Cyclic voltammograms of [**2**H]BF_4 (left) and [**3**H]BF_4 (right) with increasing equiv of CF_3COOH (denoted on right). Overpotentials were estimated by the standard potential for hydrogen evolution from CF_3COOH in MeCN solution. *Conditions:* ~0.5 mM in CH_2Cl_2 (see experimental), 0.1M $[NBu_4]PF_6$, scan rate 0.1 V/s, glassy carbon working electrode (*d* = 3.0 mm); Ag wire pseudoreference with internal Fc standard at 0 V; Pt counter electrode.

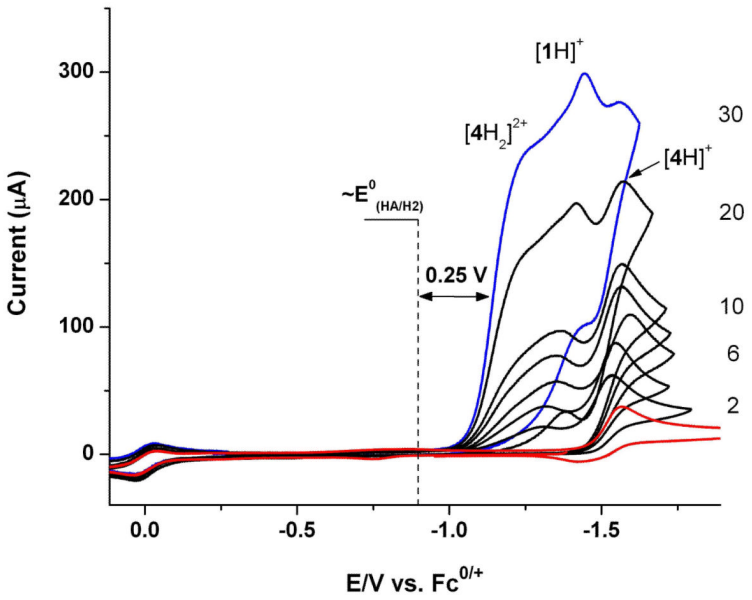

Figure 10.

Cyclic voltammograms of a CH_2Cl_2 solution (0.74 mM) of [**4**H]BF_4 with increasing equiv of CF_3CO_2H (denoted on right). *Conditions:* see Figure 9.

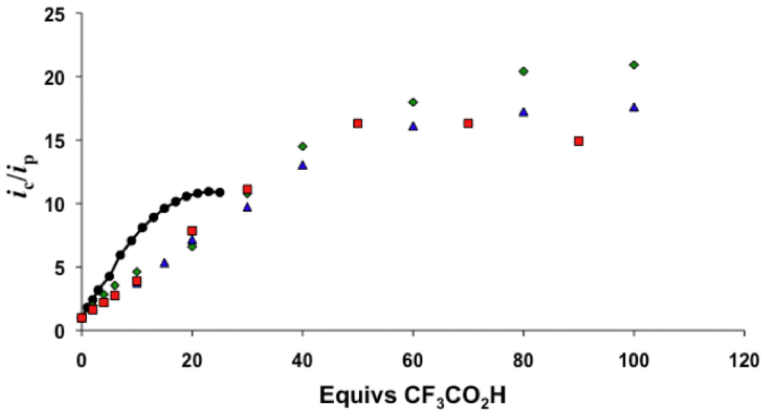

Figure 11.

Influence of [acid]:catalyst ratio on catalytic current (i_c/i_p) for [**1**H]BF_4 (black circles), [**2**H]BF_4 (red squares), [**3**H]BF_4 (blue triangles), and [**4**H]BF_4 (green diamonds). *Conditions:* see Figure 9.

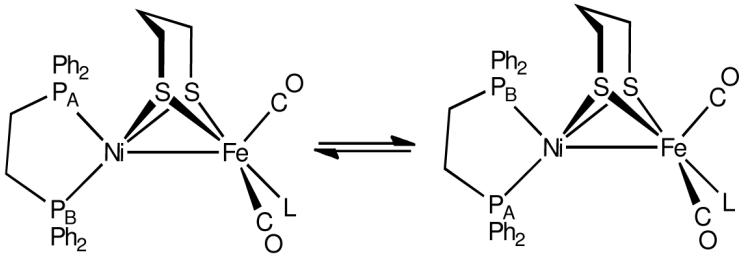

Scheme 1.
Proposed Ni-centered dynamics for **1** (L = CO) and **2** (L = $P(OPh)_3$), **3** (L = PPh_3), and **4** (L = PPh_2py).

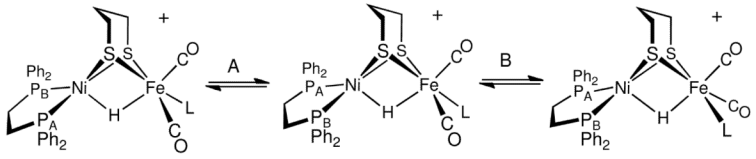

Scheme 2.

Representation of the Fe- and Ni-centered dynamic processes proposed for [**2**H]BF_4. Variable temperature ^{13}C NMR measurements indicate that pathway A has the lower barrier.

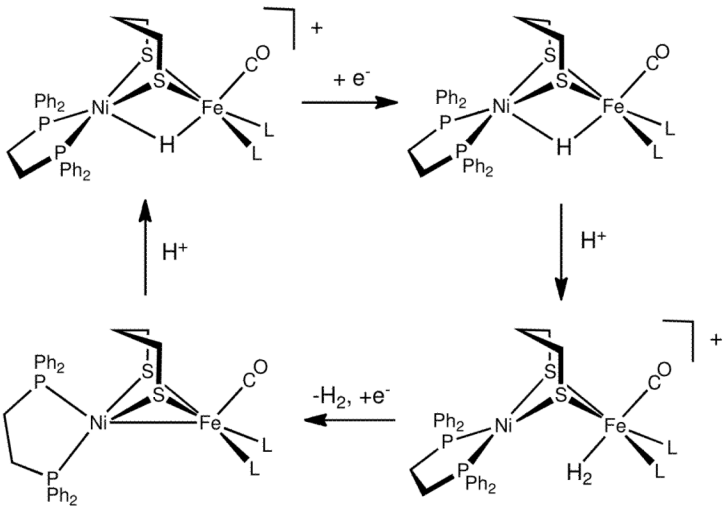

Scheme 3.
Catalytic cycle proposed for hydrogen evolution by [HNiFe(pdt)(dppe)L_2(CO)]BF_4.

Table 1

Selected Electrochemical Properties of Nickel-Iron Hydrides.[a]

Complex	$E_{1/2}$ (V) vs $Fc^{+/0}$	i_{pa}/i_{pc} (at 0.1 V/s)
[**1**H]$^+$	−1.29	0.26
[**2**H]$^+$	−1.44	0.93
[**3**H]$^+$	−1.49	0.06
[**4**H]$^+$	−1.49	0.00
[**4**H_2]$^{2+}$	−1.28	---

[a] Data were collected on ~1 mM freshly-prepared MeCN solution of nickel-iron hydride and 0.1 M $[NBu_4]PF_6$ as electrolyte.

Table 2

Thermodynamic Data (E's in V vs $Fc^{0/+}$, ΔG's in kcal/mol, NiFe = NiFe(pdt)(dppe)L$(CO)_2$).

	pK_a	E(NiFe$^{0/+}$)	E(NiFe$^{+/2+}$)	E(HNiFe$^{+/0}$)	$\Delta G_{H\cdot}$	ΔG_{H-}
[**1**H]$^+$	10.7	−0.543	−0.124	−1.29	57	79
[**3**H]$^+$	14.9	−0.722	−0.191	−1.49	58	79

J Am Chem Soc. Author manuscript; available in PMC 2011 October 27.

Table 3

Fe-H and Ni-H Bond Distances in Diiron and Nickel-Iron Dithiolato Hydrides.

Hydride	M-H Distances (Å)	Δ*d*(M-H)
$[HFe_2(pdt)(CO)_4(dppe)]BF_4$37	$(dppe)^{dibasal}(CO)$Fe-H: 1.627(3) $(CO)_3$Fe-H: 1.640(4)	0.013
$[HFe_2(pdt)(CO)_4$(NHC-chelate)$]BF_4$38	$(NHC)_2(CO)$Fe-H: 1.710 $(CO)_3$Fe-H: 1.562 Å	0.15
unsym-$[HFe_2(SC_2H_4PMe_2)_2(CO)_4]BF_4$39	$(PR_3)^{apical}(CO)_2$Fe-H: 1.59(1) $(PR_3)^{basal}(CO)_2$Fe-H: 1.74(1)	0.15
cis-$[HFe_2(pdt)(CN)(CO)_4(PMe_2)]BF_4$40	$(PMe_3)^{basal}(CO)_2$Fe-H: 1.63(1) $(NC)^{basal}(CO)_2$Fe-H: 1.70(1)	0.07
$[HNiFe(pdt)(dppe)(CO)_3]BF_4$14	Fe-H: 1.46(6) Ni-H: 1.64(6)	0.18
$[HNiFe(pdt)(dppe)(PPh_3)(CO)_2]BF_4$	Fe-H: 1.49(3) Ni-H: 1.89(3)	0.4

Table 4

Selected Catalytic Properties of the Hydrides. *Conditions:* see Experimental.

Catalyst	E_{cat}[a] (V, vs $Fc^{0/+}$)	Rate[b] (s^{-1})	Overpotential[c] (V)
[**1**H]$^+$	−1.20	20	0.31
[**2**H]$^+$	−1.32	50	0.43
[**3**H]$^+$	−1.30	50	0.41
[**4**H]$^+$	~−1.3	50	~0.4
[**4**H_2]$^{2+}$	−1.15	50	0.26
[NiFe]-hydrogenase (*A. vinosum*)	−0.345 (pH 7.4)[d]	~500[e]	~045

[a] For [**1**H]$^+$ through [**4**H]$^+$, potential at $i_{pc}/2$ for an acid-independent voltammogram.26 Potentials can be corrected from $Fc^{+/0}$ (MeCN) to NHE using the relation $E^{NHE} = E^{Fc} + 0.717$ V.46

[b] Estimated from acid-independent region of i_C/i_p vs [acid] plot.

[c] Calculated using the relation $Overpotential = E^{cat} + 0.89$ V.26

[d] Onset potential, 40 °C, vs NHE.47

[e] Lower limit estimate, 30 °C, pH 6.